Bioenergetic modeling reveals opposing effects of ocean and terrestrial warming of an intertidal crustacean

Running Title: Opposing effects of air and water warming

Emily A. Roberts[1,2], Gordon T. Ober[1,3], and Sarah E. Gilman[1]

[1] W. M. Keck Science Department of Scripps, Pitzer, and Claremont McKenna Colleges, Claremont, CA USA

[2] Current Address: School of Marine and Atmospheric Sciences, Stony Brook University, Stony Brook, NY USA

[3] Current Address: Environmental Science Department, Endicott College, Beverly, MA USA

Corresponding author

E-mail: molly.a.roberts@gmail.com

Keywords: climate change; intertidal; cirripede; thermal ecology; Scope for Growth, bioenergetic model, shore height, *Balanus glandula*

Abstract

Organism-level bioenergetics models (OBMs) are an emerging tool for predicting consequences of climate change on organism growth in ecological systems. Global changes in ocean and atmospheric temperature may affect organisms that experience both environments, such as those living in intertidal systems. The acorn barnacle, *Balanus glandula*, is prevalent throughout the intertidal zone in the Eastern Pacific, and laboratory experiments demonstrate that feeding rates and metabolic costs are sensitive to temperature. We ask, based on these thermal responses, do aerial and aquatic warming decrease *B. glandula* growth in a field environment because of increased costs and reduced feeding? We measure environmental conditions (aerial and aquatic temperature) at three intertidal heights over two 6-month intervals and compare growth estimates based on an OBM to observed growth. Initial work indicates that growth is less sensitive to elevation than predicted by lab-based physiological rates alone, so we estimate an elevation-dependent compensation factor (Z) when fitting the model to all three elevations and the two intervals. This full model predicts that, in this environment, aquatic warming will counteract increased costs of aerial warming, by virtue of increased feeding at warmer temperatures. This work advances OBMs by combining the effects of multiple decoupled thermal responses (e.g. feeding, respiration) in multiple contexts (aerial, aquatic), drawing on established model selection and "divide and conquer" techniques, and identifying sources of uncertainty in the model. This work indicates that future intertidal OBMs may benefit from an improved characterization of feeding behavior, including empirical estimates of elevation-dependent feeding compensation.

Introduction

Organism-level bioenergetic models (OBMs) are emerging tools that predict species' responses to climate change [1–3]. OBMs model an organism's energy needs as a function of abiotic conditions, physiology, and species interactions to predict organismal growth and survival. There are several different OBM frameworks, including Scope for Growth [4], the Wisconsin fish bioenergetics model [5], Dynamic Energy Budget modeling (DEB) [6], the Metabolic Theory of Ecology [7–9], and other agent-based physiological energy budget models (ABMs) [10–12]. As mechanistic models, OBMs are better suited to predicting responses under the novel combinations of environmental conditions that will occur under climate change than simpler, correlational approaches such as species distribution models [1,11]. A successful OBM must accurately capture environmental, physiological, and behavioral processes at the appropriate temporal and spatial scales. The temperatures an organism experiences can vary over hourly, daily, seasonal, and annual timescales [13], and the choice of timescale affects model predictions [14]. Temperature, in turn, affects a wide range of physiological [15,16] and behavioral processes [17–19]. Importantly, each of these processes within an organism may have its own thermal dependence [11,15,20,21].

To have confidence in a model's climate change predictions, it must be validated against empirical environmental and organismal data [11,22,23]. Model validation in more than one location or against multiple combinations of empirical conditions is essential, since models that perform well at one location or time can fail in other conditions [24,25]. Testing often reveals

poor agreement between model predictions and independent data [e.g. 22], but such tests provide an important opportunity to identify mechanistic details that can improve models [23,26]. Model validation should also include testing the sensitivity of the model to parameter uncertainty, as this can identify areas where better empirical estimates of parameters would improve model prediction [5,27,28].

Modeling decisions must be informed by the environment, or ecological niche, experienced by the study species [29]. Warming and increased frequency of marine heat waves are associated with shifts in marine communities at the land-sea interface [30,31]. Intertidal species experience two distinct thermal environments, aquatic and terrestrial, that alternate with the oscillation of tides. Individuals at higher elevations on a shore experience a shorter duration of submerged conditions, producing steep environmental gradients of temperature, desiccation and feeding opportunities [Fig. 1; ,18,25]. They often experience greater acute physiological stress [32,33] and decreased growth and reproduction [34,35]. Given that terrestrial and marine environments are expected to warm at different rates [36,37], an organism's shore height will also affect its overall experience of climate change [38]. Further, individual species may differ in their sensitivity to warming in the two environments [39]. Representing such a dynamic thermal environment, where large shifts in temperature occur multiple times daily [40], and where physiology varies with medium [41], requires a model with high-resolution timesteps [25,42–45] and separate physiological dynamics in each environment (Fig. 2a,b).

Figure 1 A) Abiotic conditions vary with the duration of low tide exposure at each shore height. B) Violin plot of daily time emerged (exposed to air) at three different shore heights.

88

89 **Figure 2** Intertidal animals alternate between submergence under water (A) and emergence in air
90 (B), each with a distinct set of physiological conditions and processes. These can be captured in
91 a Numerical Scope for Growth model (C), if timesteps are high enough resolution to capture the
92 tidal fluctuations.

93

94 Scope for Growth (SFG) models are a class of OBMs that predict organismal growth and
95 reproduction by quantifying the effects of environmental conditions and size-scaling
96 relationships on physiology [46–50]. While SFG models were originally designed to calculate
97 energetics and growth from mean conditions over long (e.g. annual) intervals, more recently,
98 Numerical SFG ("NSFG", Fig. 2C) models have been developed to capture shorter time steps
99 [51,52]. The shorter timesteps allow for energy fluxes to change allometrically as organisms
100 grow [52]. A central advantage of SFG and NSFG models is their use of empirically-derived
101 thermal sensitives [5,47], rather than assuming a specific theoretically-derived relationship
102 between temperature and physiology [6,7]. This allows for separate physiologies in air and
103 water [e.g., 50] and for separate thermal sensitives of energy demand and energy acquisition. The
104 latter is ignored in some OBM modeling frameworks [e.g., 6; but see,51–53], despite strong
105 empirical evidence for its need [20,54,55]. Further, SFG and NSFG models' rely on independent,
106 empirically-estimated parameters, each with well-characterized uncertainty. This allows for more
107 straightforward sensitivity analyses and model skill assessment than some more complex
108 modeling frameworks [27,56].

109

Here we develop an intertidal OBM model of the barnacle, *Balanus glandula,* using a hybrid of NSFG and other modeling approaches. This sessile crustacean is native to the Pacific coast of North America (Mexico to Alaska) [57] with a wide vertical distribution [58]. We model the growth of *B. glandula* across an environmental gradient, shore height. We first develop this model from empirical studies of *B. glandula* growth and physiology. We then validate the model with two six month field observations of barnacle growth at three shore heights. Our objectives are to (1) build the OBM model for *B. glandula* and test it across an environmental gradient, (2) test the sensitivity of the model's predictions to parameter uncertainty, and (3) predict the effects of future warming of air and water temperatures on *B. glandula's* SFG across its vertical range.

Methods

The traditional Scope for Growth model

Scope for Growth (SFG) models [59,60] convert physiological rates into energy equivalents and use the following equation:

$$C = P + R + U + F \quad \text{eq. 1}$$

Where *C* is the total consumption of energy from food, *P* is the production of both somatic and gonadal tissues, and R is the energy expenditure measured in terms of respiration. Additional energy is lost in the excretion of nitrogen waste (*U*) and feces (*F*). We assumed *U* was zero because Wu and Levings [50] found very little energy lost to excretion in *B. glandula*. The production of tissue (*P*) may then be estimated as the difference between energy assimilated from the food ($A = C - F$) and energy expenditure via respiration (*R*):

$$P = A - R \quad \text{eq. 2}$$

This estimate (P) is known as the Scope for Growth (SFG).

The Numerical Scope for Growth model

We built a NSFG model (Table 1) in which energy fluxes (*i.e.*, feeding and respiration) were calculated every 15 minutes. The energy flux estimates were then used to calculate a daily net SFG and change in body size [52, Fig. 2]. We estimated daily SFG as the difference between consumption and respiration costs within each day:

$$\mathrm{SFG_{day}} = \mathrm{A_{day}} - \mathrm{R_{day}} \quad \text{eq. 3}$$

Daily SFG was used to calculate barnacle opercular length (L_{day}) over the course of each 6-month experiment. First, we calculated the daily mass at the start of the following day (M_{day+1}) as the prior day's mass plus the change in mass (ΔM_{day}). We calculated ΔM_{day} by dividing the $\mathrm{SFG_{day}}$ by the energy density of barnacle tissue (E_D, J / mg AFDW, Table 1) multiplied by 1.4 to incorporate overhead costs of new tissue growth [6].

$$\Delta \mathrm{M_{day}} = \frac{\mathrm{SFG_{day}}}{1.4 \times \mathrm{E_D}} \quad \text{eq. 4}$$

Daily length was then calculated as a function of mass estimated from *B. glandula* from the same location in the Pacific Northwest (<3mm opercular length, n=89, Palmer, 1980):

$$\mathrm{L_{day}} = 2.055921\ \mathrm{M_{day}} + 0.7912 \quad \text{eq. 5}$$

154 Table 1. Summary of model parameters and their sources.

Symbol	Parameter name	Mean and SE	Unit	Source, equations
Parameters from temperature experiments and the literature				
E_D	Energy density	22.8 ± 0.7	J / mg AFDW	Wu and Levings [50], June – Aug, 1cal = 4.184J
Temperature parameters				Supplemental Information S1, Ober et al. (2019), Ober et al. *unpublished data*
a_I	Ingestion exponent	0.05936 ± 0.02853	unitless	
c_I	Ingestion coefficient	0.00056 ± 0.00022	prey / min	
a_{R_aq}	Aquatic resp. exponent	0.08031 ± 0.04077	unitless	
c_{R_aq}	Aquatic resp. coefficient	0.00003 ± 0.00002	umol O_2/15 min	
a_{R_EXP}	Aerial expos. exponent	0.04562 ± 0.01156	unitless	
c_{R_EXP}	Aerial expos. coefficient	0.00105 ± 0.00030	umol O_2/15 min	
a_{R_REC}	Aerial recov. exponent	0.02533 ± 0.00743	unitless	
c_{R_REC}	Aerial recov. coefficient	0.02677 ± 0.00473	umol O_2/15 min	
Size-scaling exponents				Supplemental Methods, estimated from Wu and Levings (1978)
d_I	Feeding size-scaling exponent	1.88 ± 0.10	unitless	
d_{R_aq}	Aquatic resp. size-scaling exponent	1.88 ± 0.10	unitless	
d_{R_aer}	Aerial resp. size-scaling exponent	2.32 ± 0.10	unitless	
Mass vs. length				
-	AFDW size-scaling exponent (used in temperature experiment equations)	2.83 ± 0.26	unitless	Gilman et al. [62]
-	AFDW size-scaling exponent (used for small experimental barnacles, 3mm operculum length and below)	0.4864	unitless	Palmer (1980)
-	AFDW size-scaling coefficient (used for small experimental barnacles, 3mm operculum length and below)	0.7912	unitless	Palmer [61]
Model parameters estimated from the optimization				
F_H	Chlorophyll half max	0.13 ± 0.04	Chlorophyll (µg / L)	This text
z	Feeding compensation exponent	1.16 ± 0.04	unitless	This text
p_{max}	Max assimilation rate relative to size and food concentration *f* ("a" in SFG)	2.04 ± 0.11	J / tissue mg AFDW	Calculated from Nishizaki and Carrington [63]

155

156

157 *15-minute energy flux calculations*

158 We modeled the temperature and size-dependence of ingestion and respiration separately for
159 immersion and emersion periods. All fluxes followed the same general function, $b(T, L)$:

160 $$b_{x,i}(T_i,L_i) = c_x \times e^{a_x T_i} \times L_i^d, \quad \text{eq. 6}$$

161 where x refers to a specific energy flux in either an air or water medium: ingestion (b_I) or
162 respiration (b_{R_AER}, b_{R_Recov}, b_{R_AQ}), and i refers to the 15-minute interval. T is the temperature, L
163 is the body size (operculum length, mm), d is an allometric length-scaling exponent, and a_x and
164 c_x are constants for the individual flux equations, fit from laboratory data (Table 1). We fit four
165 separate flux equations (Ingestion, Aquatic Respiration, Aerial Respiration, Aerial Recovery,
166 Table 1) to laboratory collected data (Supplemental Methods) [64]. The size scaling parameters
167 (*d)* were sourced from the published literature (Table 1, Supplemental Methods). Exponential
168 temperature scaling equations were selected (eq. 6) after first comparing the fit of 5 different
169 thermal scaling equations to the laboratory-collected data (Supplemental Methods) [65].

170

171 We calculated energy assimilation (A_i) at each time point from the ingestion flux ($b_{I,i}$),

172 $$A_i = p_{max} \times \frac{F_i}{F_i - F_H} \times b_{I,i}(T_i,L_i) \quad \text{eq. 7}$$

173 Where p_{max} is the maximum ingestion rate, and $b_{I,i}$ is the ingestion of the organism as a function
174 of T_i and L_i (eq. 6). Food availability ($f = \frac{F_i}{F_i - F_H}$, unitless), is a Holling's Type II functional
175 response where F_i is chlorophyll concentration at time i, and F_H is the chlorophyll concentration
176 at half of the maximum ingestion rate [6].

177

178 *Additional modifications for an intertidal species*

179 Additional modifications of the NSFG model were needed to accurately reflect intertidal
180 dynamics. First, we used separate energy demand equations during immersion and emersion that
181 reflected their differing thermal sensitivities. We further calculated the metabolic cost of aerial
182 exposure as the sum of measured respiration during emersion (b_{R_EXP}) plus additional recovery
183 costs ("oxygen debt") upon resubmersion [64,b_{R_REC} 66]. Daily energy demand values were then
184 calculated as a daily sum of the 15-minute timesteps:

185 $$R_{\mathrm{d}} = \sum_{i=1}^{96} \mathrm{R}_i, \quad \mathrm{R_i} = \begin{Bmatrix} \mathrm{WL}_i \geq \mathrm{elev} \\ \mathrm{WL}_i < \mathrm{elev} \end{Bmatrix} \middle| \begin{matrix} b_{\mathrm{R\_AQ},\,i} \\ b_{\mathrm{R\_EXP},i} + b_{\mathrm{R\_REC},i} \end{matrix} \qquad \text{eq. 8}$$

186 where WL_i is the water level at timestep i and *elev* is the elevation or height on the shore of the
187 modeled barnacles.

188

189 Second, assimilation was calculated under immersion using Eq. 7, but during emersion
190 assimilation was considered to be negligeable. Daily assimilation values ($\mathrm{A_d}$) were then
191 determined from the summation of assimilation estimates at 15-minute timestep:

192 $$A_{\mathrm{d}} = \sum_{i=1}^{96} \mathrm{A}_i, \quad \mathrm{A}_i = \begin{Bmatrix} \mathrm{WL}_i \geq \mathrm{elev} \\ \mathrm{WL}_i < \mathrm{elev} \end{Bmatrix} \middle| \begin{matrix} \mathrm{A}_i \\ 0 \end{matrix} \Bigg\}. \qquad \text{eq. 9}$$

193 Last, we added a tidal compensation term S^z (Table 1) to the feeding flux to allow for greater
194 rates of consumption at higher shore heights. Here S is the proportion of time submerged over
195 the entire period of the model. Without this term, the model would assume energy intake
196 declines linearly as a function of submergence times at higher shore heights. Yet many intertidal
197 species [34,67,68], including *B. glandula* [69] compensate for reduced submergence with greater

feeding activity and/or larger feeding structures. Initial model runs without this term severely underestimated growth at higher shore heights and overestimated growth at lower shore heights.

$$A_{elevation,i} = A_i \times S^z \quad \text{eq. 10}$$

Observational study site

Field temperatures and barnacle growth were recorded on a Southwest-facing rock wall at the University of Washington's Friday Harbor Laboratories Biological Preserve (FHL), San Juan Island, WA (48°32'45.1" N, 123° 0' 39.2" W) in the Salish Sea. This region is characterized by mixed semi-diurnal tides, and experiences its greatest low tide temperatures in the summer, when daytime low tides are most common [58]. Local water temperatures average ~10°C annually [64].

Biological observations

Thirty-three 13.5cm x 13.5cm photoquadrats were established along the rock wall as part of a larger study of *B. glandula* growth across multiple latitudes (Gilman et al., *unpubl. data*). At each of three shore heights (1.20m, 1.55m, and 1.97m + MLLW), we spaced eleven quadrats in a horizontal row approximately 1.5 m long. The three heights spanned the upper and lower limits of *B. glandula* on the wall. We photographed each quadrat in February 2018, August 2018, and March 2019. At each time point, a PentaxK50 digital SLR camera was placed 16 cm above the quadrat. The opercular length of *B. glandula* was measured as the maximum operculum diameter on the digital images using ImageJ (v.1.5) [70]. Growth was calculated as the change in opercular length between each pair of time points. All analyses were restricted to the smallest

barnacles (1.5mm – 3mm initial opercular length) to maximize our ability to detect growth and to ensure that we used an independent set of barnacles for each growth period.

Environmental observations

To estimate barnacle body temperature during both emersion and immersion, three temperature dataloggers (Onset Hobo TidbiT v1 and v2) were deployed within each shore height and recorded temperature every 15-min from February 2018 – March 2019. Temperature loggers were attached to the rock face within individual quadrats using z-spar epoxy. We averaged the replicate loggers within a shore height to reduce the effect of thermal microhabitat variation [71]. Tidal elevation was determined by comparing seawater temperature and 6-minute tide gauge data (National Buoy Data Center Station FRDW1 - 9449880, NOAA National Ocean Service, ndbc.noaa.gov/station_page.php?station=frdw1) to the 15-minute temperature logger data. Weekly averages of seawater chlorophyll fluorescence were calculated from the Padilla Bay Gong Site, WA (48° 33' 26.9" N, 122° 34' 19.2" W) and used to estimate food availability (YSI EXO-2 sonde, Chl μg/L, NERRS CDMO PDBGSWQ, 2017 - 2020).

Energy flux parameters

We used laboratory-collected data [50,64; G. Ober *unpubl. data*] to fit the energy flux equations $b_{R\_AQ}(T, L)$, $b_{R\_EXP}(T, L)$, and $b_{R\_REC}(T, L)$ $b_I(T, L)$ (eq. 6, Supplemental Methods). Given that these studies were performed over a narrow range of body sizes, the size-scaling exponents $d_{AQ,}$ $d_{AER,}$ and d_I were derived separately from equations reported by Wu and Levings [50] for *B. glandula.* For energy demand, we converted the laboratory-measured respiration rates to joules by multiplying by 0.457 J µmol O_2 L^{-1} [64,72,73].

243

244 *Model fitting*

245 We used a two-step optimization method to estimate three model parameters (p_{max}, z, F_H) on
246 independent subtidal and intertidal datasets. First, we determined the maximum assimilation rate
247 p_{max} by fitting the model to observed *B. glandula* growth over 5 weeks in subtidal conditions,
248 using data from Nishizaki and Carrington [63]. To account for a lag in growth, we used
249 chlorophyll values from 2 weeks prior to each growth timestep [74].

250

251 Second, we estimated the feeding compensation parameter (z) and the feeding half saturation
252 coefficient (F_H) by fitting the full model to the 291 intertidal barnacle growth measurements
253 across the three elevations and two-time intervals (n=10-107 growth measurements per elevation
254 and timepoint combination).

255

256 For both optimizations, the growth of individuals from the photo quadrats was compared with
257 model predictions of growth. Final length L_{final} was determined estimated from the numerical
258 model. The initial length of each replicate sample (L_{init}) was the initial length of each barnacle
259 from the photo quadrat, and the model estimated length (L_{day}) each day based on SFG, iterating
260 for each day of the 6-month dataset. The predicted growth ΔL_{pred} was calculated for each
261 replicate barnacle as the difference between the final (L_{final}) and initial lengths (L_{init}). We solved
262 for the values of $p_{max,}$ z, and F_H that gave the lowest negative log likelihood of the data given the
263 model, optimizing for the sum of $\Delta L_{pred} = \Delta L_{obs}$ for all barnacle growth measurements.

264

Statistical and numerical analysis

All statistical analyses and numerical modeling were performed in R (v4.0) and RStudio (v1.3). The model optimization minimized the sum of the negative log likelihoods (NLLs) of the data given the model for each tidal elevations and season. NLL estimations assumed a normal distribution. A bounded BFGS algorithm was used for the maximum likelihood estimation (optim package in R). The hessian matrix was used to estimate approximate standard error of the parameters.

Sensitivity analysis

The sensitivity analysis of the NSFG model was modified from the individual parameter perturbation (IPP) approach [e.g., 5]. Rather than determining the sensitivity to a percentage change in the absolute value of each parameter, we determined the sensitivity to a change of one standard error (±1 SE) in each parameter value [75] This method was used to capture the sensitivity of the model relative to a realistic range of uncertainty in parameters values [76] rather than a fixed percentage of the mean. The standard error of each parameter value was determined from either the published literature or from our empirical parameter fits (Table 1). A sensitivity of 1.5 indicates that a change in the parameter by 1 SE causes a resulting change in the SFG by 50%.

Climate change estimation

The effect of ocean and aerial warming on cumulative SFG (J) was determined over each 6-month interval for a barnacle of an initial size of 2.2 mm at each elevation. Seawater and/or aerial warming was estimated by adding a discrete integer value from 0 to 2°C (seawater) and/or

0 to 4°C (aerial warming) to every 15-minute observation of estimated body temperature during immersion and emersion. We chose these ranges because they encompassed the range of abiotic warming expected in the Salish Sea in the year 2095 relative to 2000 under the Representative Concentration Pathway 8.5 emissions scenario (RCP8.5) [36].

Results

Environmental and biological observations

Weekly averaged chlorophyll ranged from 0 to 18 μg / L and was highest in June. Measured water temperatures at the field site ranged from 5°C to 17°C, and low tide temperatures ranged from -3°C to 31°C. Aerial exposure occurred 72% of the year at the highest elevation, 48% at the mid elevation, and 33% at the lowest elevation (Fig 1b, 3a-c, 4a-c). The low shore height experienced consistently cooler aerial temperatures than the other two shore heights (Fig 3d-f, 4d-f). However, the mid shore was often warmer at low tide than the high shore, due to a rock overhang that shaded some of the high shore quadrats. Generally, the warmest aerial temperatures occurred in August, while the coldest were in February.

Figure 3. Model inputs and predicted barnacle growth for 3 shore heights over interval 1 (Feb-Aug 2018). A-C) Proportion of the day submerged and food availability (*f*) in the low, middle, and upper intertidal zone during the first interval. D-F) Mean daily temperature during aerial (solid purple line) and aquatic (solid blue line) conditions and daily 75% quantile of temperature (dotted red line). G-I) Daily physiological intake (dark green), aerial cost (purple), and aquatic cost (blue) of a barnacle of 2mm initial operculum length. The aerial cost includes both aerial

exposure and aerial recovery costs. J-L) Daily Scope for Growth of a representative barnacle of ~2mm.

Figure 4. Model inputs and predicted barnacle growth for 3 shore heights over interval 2 (Aug 2018- Mar 2019). See Figure 3 for details.

Small barnacles (mean initial size 2.2 mm) grew 0.5 to 0.8 mm in operculum length over 6 months depending on the time interval and shore height (Figure 5, x-axis). Individuals in the low intertidal tended to grow 34 and 40% more than those the upper intertidal in intervals 1 and 2, respectively (Figure S2.1), but this difference was not statistically significant (Table S2.1). The narrow range in mean growth rates contrasted with the large range in time submerged across the three shore heights (Figure 1b).

Figure 5. The relationship between predicted growth and observed growth in mm at the three elevations (Low – blue, mid – orange, upper – grey) in interval 1 (closed circles) and interval 2 (open circles, means ± SE).

Model Fit

Predictions from the NSFG model matched mean observed growth fairly well ($R^2 = 0.76$), with the largest model discrepancies in the low intertidal, which had the fewest samples (Figure 5). There was also a large amount of inter-individual variation in growth within each time point and shore height, and individual growth was not well predicted by the SFG model ($R^2 = 0.07$, data

not shown). Representative trajectories of energy fluxes in aerial and aquatic conditions over the course of a day for each elevation are shown in Supplemental Figure S2.2.

Parameter estimation

Based on the subtidal analysis, we found p_{max}, the size-dependent maximum assimilation rate was 2.0 ± 0.1 J normalized per mg of tissue (AFDW, Table 1). The chlorophyll half-saturation coefficient, fit on the intertidal growth data, was low (F_H = 0.13 ± 0.04 μg Chl / L), relative to the observed chlorophyll concentrations. Consequently, the model predicted feeding and ingestion (*f*) to remain over 80% of the maximum ingestion rate throughout the study (Figure S2.3, Fig 3a-c, Fig 4a-c). The feeding compensation exponent, z, was estimated as 1.16 ± 0.04, which corresponds to a three-fold increase in feeding activity for barnacles at the high shore height compared to those at the low shore height (Table 1, Figure 6).

Figure 6. Estimated feeding activity in the upper (square), mid (circle), low (triangle) tidal elevations as a function of the proportion of time submerged over each 6-month interval (interval 1 – open symbols, interval 2 – closed symbols). Feeding activity at each elevation is calculated as an exponential function of the proportion of time submerged (S) over the full 6-month interval, $y = S^z$ ($z = 1.16 + 0.04$, mean + SE, Table 1).

Daily energy fluxes and predicted Scope for Growth

Daily energy intake and costs followed the daily patterns in submergence time. On days with more time emerged aerial costs increased, while feeding and aquatic costs increased on days with more time submerged. As barnacles grew over each 6-month period, all energy fluxes increased

(Fig 3G-F, 4G-F). Interestingly, barnacles in the low intertidal exhibited the greatest energy intake even after including feeding compensation in the model (Fig. 7, Supplemental Figure S2.4). For animals at higher shore heights, the decreased time in aquatic conditions yielded a decrease in immersion costs and an increase in emersion costs (Figure 7). Overall, predicted SFG increased over time across all elevations. Interestingly, except for the low shore (Fig 3J, 4J), SFG was not monotonic with time. In the upper intertidal, the cumulative SFG initially decreased in September, a period of low submergence durations and warm aerial temperatures, before increasing later in the interval (Figure 4L).

Figure 7. Violin plots of daily energy fluxes at each tidal elevation for interval 1 (A) and interval 2 (B). Cumulative intake (green), aquatic cost (blue) and aerial cost (purple). Aerial cost is the sum of exposure and recovery costs.

Model sensitivity to parameter estimates

The individual parameter perturbation (IPP) found that the SFG (J) was most sensitive to uncertainty in the temperature parameters for feeding, followed by aerial and aquatic respiration (Figure 8). Increasing the feeding coefficient (c_I) and feeding temperature exponent (a_I) by each parameter's empirical standard error (SE) had the largest effect on predicted SFG. A one SE increase in c_I resulted in a 300% increase in SFG, while a one SE increase in a_I led to a 260% increase in SFG. Increasing the aquatic and aerial respiration coefficients (a_{R_aq} and a_{R_aer}) by one SE caused a ~ 80% decrease in SFG. In contrast, SFG was minimally sensitive to changes in the energy density parameter (E_D, J mg^{-1}) and in the size scaling parameters for all energy fluxes (d_I $d_{R\ aq}$, $d_{R\ aer}$). SFG was also more sensitive to the aerial exposure parameter uncertainty ($a_{R\ EXP}$,

$c_{R\,EXP}$) compared to the aerial recovery parameter uncertainty ($a_{R\,REC}$, $c_{R\,REC}$). Finally, the variability of the SFG estimate due to the variability in initial body size was 40% (population SE, Pop_{SE}, Figure 8).

Figure 8. Sensitivity analysis representing the influence of parameter uncertainty on cumulative barnacle SFG (J) over 6 months (see Table 1 for parameter definitions). The sensitivities are for the SFG of a representative barnacle in the mid elevations in interval 1 (Feb – Aug), and the Pop_{SE} is the population uncertainty among the barnacles in the middle elevation.

Warming body temperatures and SFG

Warming body temperatures during emersion decreased predicted growth by 10-30% per 1°C increase, depending on the shore height and time interval, while warming during immersion increased predicted growth by 15-40% per 1°C (Fig 9). For example, in the mid shore, a 2°C increase in aerial body temperatures resulted in a 30-50% reduction in SFG, while a 2° C increase during immersion increased predicted SFG by 40-60%. Thus, when body temperatures warmed similar amounts in air and water there was almost no change in predicted growth.

In scenarios that remained below 2°C warming, SFG remained high in the low shore sites (>70 J), with only a 17-23% decrease in predicted growth due to warming aerial body temperatures. Both the cost of aerial warming and the benefit of warming during immersion were greater in the upper intertidal, where 4°C aerial warming alone caused the SFG prediction to drop to near or below 0 (-7 to 12J). However, when that aerial warming was combined with 2°C aquatic

warming, the high shore SFG remained above 0, and within 30-50% of the present day SFG prediction.

Figure 9. The influence of increased body temperatures during aerial and aquatic exposure on cumulative barnacle SFG (J) over 6 months in the upper (A, B), mid (C, D), and low (E, F) elevations in interval 1 (Feb – Aug; A,C,E) and interval 2 (Aug – Feb; B,D,F) for a theoretical barnacle of 2.2 mm initial operculum length. The SFG for the observed environmental temperatures (Δ°C = 0; lower left quadrant of each 3X3 square) ranged from 40 to >100 J.

Discussion

Successfully predicting the effects of warming temperatures from climate change on species requires building physiologically accurate, field-tested models of organismal responses to warming temperatures [1,77]. Here we developed a Numerical Scope for Growth (NSFG) model for the intertidal barnacle *Balanus glandula* and used it to predict the effects of warming body temperature during high and low tide. The model explained 76% of the variability in growth across the three intertidal shore heights and two time periods, after adding a new parameter for feeding compensation. We found that increasing body temperatures during immersion buffered the negative effects of increased air temperatures at low tide. Specifically, higher aquatic body temperatures increased growth by increasing feeding rates during immersion more than they increased energy costs, while warming aerial body temperatures reduced growth by increasing costs without changing feeding. The NSFG model demonstrated a new method for developing and testing OBMs that used high resolution timesteps, independent curve fits for different energy

fluxes, and estimated one parameter, rather than many, with an independent subtidal growth dataset [11]. However, our findings are contingent on the accuracy of the laboratory-measured parameters for feeding and energy demand. Our sensitivity analysis showed that lab-based predictions of growth were greatly influenced by the uncertainty in the relationship between temperature and feeding. Finally, this work highlights the importance of model testing and sensitivity analyses to identify information gaps and form new hypotheses that can improve future models.

Warming body temperatures and barnacle SFG

Our model suggests that *B. glandula* will respond very differently to warming body temperatures at high and low tide. Warming during submersion enhanced growth while warming during emersion reduced growth (Fig 9). When submerged, the energetic costs of warming were offset by larger gains in energy intake. In contrast, emersion warming could only influence costs. This effect was greatest on the low shore, where Scope for Growth increased with warming as long as the magnitude of aerial warming did not exceed aquatic warming (Fig 9E,F). In contrast, warming on the high shore only led to increased growth when aquatic warming was greater than aerial warming (Fig 9A,B). Interestingly, shore height also influenced the relationship between SFG and aerial warming, as the same amount of aerial warming depressed SFG more on the high than the mid shore, even though the mid-shore had warmer emersion temperatures overall.

Importantly, terrestrial rates of warming are predicted to exceed marine warming, a phenomenon known as the "land-sea warming contrast" [78]. In the Salish Sea, average air temperatures are predicted to increase by 3.5C by 2095 under RCP 8.5, more than double the predicted sea surface

444 temperatures warming of 1.57°C [36,37]. At this 2:1 warming ratio of emersion to immersion,
445 our model predicts up to a 40-70% decrease in SFG at the higher elevation, and a 10-40%
446 decrease in SFG at the lower elevation, depending on the time interval.
447
448 These results suggest that the negative effects of climate warming are likely to be greatest on the
449 high shore. If this is the case, *B. glandula* could experience a vertical contraction of its upper
450 limit, due to negative Scope for Growth (Figs. 3,4) [79], even as individuals lower on the shore
451 continue to thrive. Indeed, Harley [30] has already documented an average 40cm drop in the
452 upper vertical limit of *B. glandula* over 50 years at 20 sites within the Salish Sea. However, the
453 relationship between survival and energetics is complex [80]. These vertical range contractions
454 could also be driven by changes in the frequency of acute lethal events [81] or changes in other
455 low tide stressors, such as desiccation [82], rather than a sustained negative Scope for Growth.
456 Further, our study animals were 2-3mm opercular length, but earlier life stages could be more
457 susceptible to abiotic stressors at high elevations [83]. Additional research is needed to determine
458 the relative importance of these different mechanisms of stress, including interactions, to
459 intertidal species distributions. It is also worth noting that, while intertidal animals will
460 experience the full amount of aquatic warming, aerial body temperature warming is often much
461 less than the full amount of abiotic aerial warming [38,84]. If barnacle body temperatures during
462 emersion warm more slowly than air temperatures, barnacles will be less negatively impacted
463 than we predict here. Accurate predictions of barnacle body temperature warming at low tide
464 will require detailed biophysical modeling [38,77].
465

Intertidal organisms in the Salish Sea, including *B. glandula*, occupy a unique thermal niche. In this region, *B. glandula* experience some of the coldest immersion temperatures anywhere in its geographic range and some of the warmest emersion body temperatures [85]. It is unclear how generalizable the benefits of warming aquatic temperatures observed here are to other populations of *B. glandula* or to other intertidal species. Experimental studies of other Northeastern Pacific intertidal species, have found an increase in feeding rates under warming water temperatures for some snails [86–88], seastars [86] and barnacles [39], but increases in feeding do not always translate into increased growth [86]. Moreover, different populations of a species can vary in their response to temperature [88]. The relationship between growth and temperature can also be influenced by species interactions, such as non-lethal predator effects on prey [39,89]. Further, species that regularly experience temperatures near and above their thermal feeding optima, or that live in environments in which temperature modulates local biogeochemistry may be especially vulnerable to the combined effects of aerial and water warming [90]. Thus, while some intertidal species may experience the benefits of warming water temperatures under specific conditions, those conditions may be idiosyncratic to specific populations and/or ecological situations.

Advantages and limitations of our Numerical Scope for Growth approach

One of the central challenges of modeling organismal responses to climate change is designing models that capture physiology and environmental conditions at appropriate levels of detail [40,77]. A multitude of organism-level bioenergetic models have been proposed [5,6,9,46]. We used a hybrid modeling approach that combined a short time-step Numerical Scope for Growth model with elements of several other approaches (Fig. 2, Table 1). Our OBM model estimated

growth daily, which is a much shorter timestep than traditional SFG models, and relied on temperature data at an even shorter timestep (15 minutes) to accurately capture the dynamic tidal environment of *B. glandula*. The model also incorporated key ideas from DEB models, including a nonlinear function of feeding rate relative to food concentration [6,52] and a 40% overhead cost for growth [6].

One major difference among OBM frameworks is the number of distinct thermal sensitivities incorporated into the model for different aspects of an organism's physiology, such as consumption and metabolism. At one extreme, all thermal sensitivities in DEB and MTE are modeled with a single equation derived from theoretical principles [6,7], although some applications of these models allow individual parameters to vary by physiological process [e.g., 9]. In contrast, fish bioenergetics and SFG models typically incorporate unique thermal sensitivity equations for each process and fit these equations from empirical data [5,e.g., 47]. We chose the latter approach, because of a growing consensus that energy consumption and energy demand exhibit different thermal sensitives [11,20,55]. We fit four distinct curves: feeding, aquatic energy demand, aerial energy demand, and aerial recovery (oxygen debt). In fitting thermal sensitivity equations to empirical data, there are a wide range of curves to choose from [8,91,92]. We used an information theory approach to compare 5 representative curve formulations (Supplemental Methods). In fitting the curves, we drew on empirical datasets that contained a wide range of temperatures, well beyond what this species currently experiences (aerial: 5-38°C, aquatic: 5-26°C), to ensure the model would be relevant for novel environmental conditions [11].

Divide and conquer strategies integrate sub-model simulations with top-level simulation experiments with the aim of assessing research questions with more valid and realistic simulations [11,93]. Many bioenergetics models include sub-model growth simulations within the preparatory stage [26,94,95]. Importantly, we used a sub-model growth simulation to estimate two parameters, only one of which was then integrated into the top-level model. Specifically, this sub-model simulation was an independent dataset of barnacle growth in a subtidal environment (no immergence). This sub-model simulation was used to estimate maximum assimilation rate p_{max}. Then, the top-level experiment investigated whether the model predicted growth across three tidal elevations and two time periods. When this model failed to converge, we tested a new quantitative hypothesis, that feeding varied exponentially with tidal elevation, and we then tested this against all three tidal elevations and two time periods. This strategy allowed us to use one parameter (z) to account for the discrepancy between predicted growth based on the model vs. observed growth.

Within a statistical model, only some parameters have scientific interest. In such models, "nuisance parameters" address random mechanisms, and variability resulting from them, but have no intrinsic value in themselves [96]. The half-saturation coefficient is used in NSFG and DEB models [6,52], and allows for saturation of feeding at high food densities which is more realistic [97,98]. Here, the half saturation coefficient for feeding (F_H) was estimated once, independently for each of the sub model and top level model. In DEB models, this coefficient is calculated for each location separately [6]. This method of validation in place of independent model testing is difficult to avoid since this variable is associated with food quality and is difficult to characterize empirically [6], and may vary by location [24,25]. In our study, the three

shore heights were within a meter of one another. While it's plausible that food quality may have varied across the 6-month experiment, this work makes strategic use of a system in which food quality across space is a reasonable assumption. The half-saturation coefficient value (Table 1) constrained feeding to ~80-100% of the maximum feeding rate throughout the entire year (Fig 3a-c). Rather than considering this value as corresponding to some intrinsic value of food quality, perhaps this number is best considered a nuisance parameter that constrains the influence of the food metric on intake. In this study, a low F_H limited the influence of monthly chlorophyll on food availability (Fig S2.3).

Tidal compensation and sensitivity of the SFG estimate to feeding

One surprising result of our model was that it failed to capture growth across the tidal gradient unless we allowed feeding rate to vary with shore height. Most intertidal animals can only feed while submerged so that a shorter submergence time should shorten the time for feeding. Yet, growth differences across tidal elevation were not directly proportional to submergence time. *B. glandula* at the higher elevations were submerged ~60% less than those in the lower elevation, but their growth was only 30% less than that in the low elevation and this difference was not statistically significant (Figure S2.2, Supplemental Table S2.1). Intertidal animals can compensate for reduced submersion by either increasing feeding rates or conserving energy [34,99–101]. While not all intertidal species exhibit tidal compensation [99], 1.5 to 10-fold increases in feeding rates with elevation have been reported in *Balanus* species [68,69]. We found a 3-fold increase in feeding activity across *B. glandula*'s vertical range, which is comparable to the 6-fold increase reported by Horn et al. [69] for a central California population of *B. glandula.* Other factors, such as energy conservation at high elevations [34], species

interactions [102], or hydrodynamics [63] could also modulate relationships between submergence time and feeding activity. The need for a tidal compensation parameter highlights the importance of strategic field-testing models across multiple environments or populations [11]. A model based on only laboratory data or tested in only one environment would not have identified the need for tidal compensation.

The sensitivity analysis also identified that the SFG was most sensitive to the uncertainty in the feeding energy flux equation. Specifically, increasing the feeding coefficient by its SE increased SFG by ~3-fold. Feeding rates are highly variable and challenging to characterize given effects of particle selection, food quality, uptake of nutrients, current velocity [63], and the hiding behaviors [68] and passive vs. active feeding behaviors [69] described above. This work suggests that future lab-based growth models may be improved by focusing on more accurately characterizing feeding behavior.

Model sensitivity to parameter uncertainty

One advantage of Scope for Growth models over other OBMs is that they have a simpler structure so model uncertainty is easier to evaluate and interpret [27,28]. We used a variation on Individual Parameter Perturbation [5,76], in which we tested the model sensitivity to parameter uncertainty. This method allowed for realistic estimates of uncertainty that are scaled based on parameter uncertainty rather than the magnitude of the parameter. When parameter sensitivity is calculated in bioenergetics models, it is often based a nominal 10% change in each parameter value to investigate sensitivity to each value [5,103]. A nominal 10% change in a parameter value is sensitive to the units (e.g. °C vs. K), and may not be biologically relevant. Here, we

581 estimated the error around each parameter (SE) or obtained its SE from the literature, and
582 perturbed each parameter with this uncertainty [75]. This method may be most appropriate for
583 NSFG models and other models with simple structures that meet two criteria; First, there is little
584 to no information about the shape of the priors necessary for Bayesian analyses [27, Personal
585 communication Boersch-Supan], and second, the uncertainty of individual parameters is
586 estimated separately from independent datasets such that newer multi-tier parameter estimation
587 methods are not required to characterize parameter uncertainty [104].
588
589 *Conclusions*
590 This study presents an OBM to describe physiological consequences of changing aerial and
591 atmospheric temperatures on a rocky intertidal crustacean. We found that warming of aerial and
592 aquatic temperatures had opposite effects on the growth of the intertidal barnacle *Balanus*
593 *glandula*. The high sensitivity of the model to the relationship between temperature and feeding
594 suggests that factors affecting clearance rates, feeding, and assimilation may have a large impact
595 on growth and distribution. Our OBM applied standardized statistical methods to physiological
596 energy budgets, incorporating high-resolution environmental data and a suite of physiological
597 lab-derived data. The process of field testing models is necessary to build effective predictive
598 models that forecast the effect of climate change on marine species [11]. Such models are needed
599 to adjust marine species management and conservation efforts to dynamic and changing
600 environmental conditions [10,12].
601
602

Acknowledgements

We thank R. Rognstad, E. Hazelton, E. Carrington and M. Nishizaki for generously sharing data and providing other help. We also thank A.Gleekel, S. Malik, E. Ueland, S. Ueland, K.Roberts, E. Kovachevich, and S. Martin for their contributions to the photoquadrat dataset. Finally, special thanks to E. Pousse, E. Munroe, W. King, and R. Cerrato for feedback and insightful discussions that improved the quality of this manuscript. This work was supported by the National Science Foundation (grant IOS-1351445 to S.E.G.) with additional support from the Keck Science Department of Claremont McKenna, Pitzer, and Scripps Colleges. Any opinions, findings, and conclusions or recommendations expressed in this material are those of the authors and do not necessarily reflect the views of the National Science Foundation.

Full data citations

NOAA National Estuarine Research Reserve System (NERRS). System-wide Monitoring Program. Data accessed from the NOAA NERRS Centralized Data Management Office website: *accessed* 22 October 2020.

Literature Cited

1. Buckley LB, Cannistra AF, John A. Leveraging Organismal Biology to Forecast the Effects of Climate Change. Integr Comp Biol. 2018;58: 38–51. doi:10.1093/icb/icy018

2. Harvey CJ, Moriarty PE, Salathe EP. Modeling climate change impacts on overwintering bald eagles. Ecol Evol. 2012;2: 501–514. doi:10.1002/ece3.204

3. Troia MJ, Perkin JS. Can fisheries bioenergetics modelling refine spatially explicit assessments of climate change vulnerability? Conserv Physiol. 2022;10: coac035. doi:10.1093/conphys/coac035

4. Bayne BL, Newell RC. 9 - Physiological Energetics of Marine Molluscs. In: Saleuddin ASM, Wilbur KM, editors. The Mollusca. Academic Press; 1983. pp. 407–515. doi:10.1016/B978-0-12-751404-8.50017-7

5. Kitchell JF, Stewart DJ, Weininger D. Applications of a Bioenergetics Model to Yellow Perch (*Perca flavescens*) and Walleye (*Stizostedion vitreum vitreum*). J Fish Res Board Can. 1977;34: 1922–1935. doi:10.1139/f77-258

6. Kooijman S. Dynamic Energy Budget theory for metabolic organisation. Camb Univ Press. 2010.

7. Brown JH, Gillooly JF, Allen AP, Savage VM, West GB. Toward a Metabolic Theory of Ecology. Ecology. 2004;85: 1771–1789. doi:10.1890/03-9000

8. Bruno JF, Carr LA, O'Connor MI. Exploring the role of temperature in the ocean through metabolic scaling. Ecology. 2015;96: 3126–3140. doi:10.1890/14-1954.1

9. Vasseur DA, McCann KS. A Mechanistic Approach for Modeling Temperature-Dependent Consumer-Resource Dynamics. Am Nat. 2005;166: 184–198. doi:10.1086/431285

10. Boyd R, Thorpe R, Hyder K, Roy S, Walker N, Sibly R. Potential Consequences of Climate and Management Scenarios for the Northeast Atlantic Mackerel Fishery. Front Mar Sci. 2020;7. doi:10.3389/fmars.2020.00639

11. Rose K, Holsman K, Nye J, Markowitz E, Banha T, Bednaršek N, et al. Advancing bioenergetics-based modeling to improve climate change projections of marine ecosystems. Mar Ecol Prog Ser. 2024;732: 193–221. doi:10.3354/meps14535

12. Sibly RM, Grimm V, Martin BT, Johnston ASA, Kułakowska K, Topping CJ, et al. Representing the acquisition and use of energy by individuals in agent-based models of animal populations. Methods Ecol Evol. 2013;4: 151–161. doi:10.1111/2041-210x.12002

13. Kefford BJ, Ghalambor CK, Dewenter B, Poff NL, Hughes J, Reich J, et al. Acute, diel, and annual temperature variability and the thermal biology of ectotherms. Glob Change Biol. 2022;28: 6872–6888. doi:10.1111/gcb.16453

14. Sheldon KS, Dillon ME. Beyond the Mean: Biological Impacts of Cryptic Temperature Change. Integr Comp Biol. 2016;56: 110–119. doi:10.1093/icb/icw005

15. Dell AI, Pawar S, Savage VM. Systematic variation in the temperature dependence of physiological and ecological traits. Proc Natl Acad Sci U S A. 2011;108: 10591–10596. doi:10.1073/pnas.1015178108

16. Huey RB, Kingsolver JG. Climate warming, resource availability, and the metabolic meltdown of ectotherms. Am Nat. 2019;194: E140–E150. doi:10.1086/705679

17. Fey SB, Vasseur DA, Alujevic K, Kroeker KJ, Logan ML, O'Connor M, et al. Opportunities for behavioral rescue under rapid environmental change. Glob Change Biol. 2019;25: 3110–3120. doi:10.1111/gcb.14712

18. Hayford HA, Gilman SE, Carrington E. Tidal cues reduce thermal risk of climate change in a foraging marine snail. Clim Change Ecol. 2021;1: 100003. doi:10.1016/j.ecochg.2021.100003

19. Woods HA, Dillon ME, Pincebourde S. The roles of microclimatic diversity and of behavior in mediating the responses of ectotherms to climate change. J Therm Biol. 2015;54: 86–97. doi:10.1016/j.jtherbio.2014.10.002

20. Lemoine NP, Burkepile DE. Temperature-induced mismatches between consumption and metabolism reduce consumer fitness. Ecology. 2012;93: 2483–2489. doi:10.1890/12-0375.1

21. Monaco CJ, McQuaid CD, Marshall DJ. Decoupling of behavioural and physiological thermal performance curves in ectothermic animals: a critical adaptive trait. Oecologia. 2017;185: 583–593. doi:10.1007/s00442-017-3974-5

22. Chipps SR, Wahl DH. Bioenergetics Modeling in the 21st Century: Reviewing New Insights and Revisiting Old Constraints. Trans Am Fish Soc. 2008;137: 298–313. doi:10.1577/T05-236.1

23. Ney JJ. Bioenergetics Modeling Today: Growing Pains on the Cutting Edge. Trans Am Fish Soc. 1993;122: 736–748. doi:10.1577/1548-8659(1993)122<0736:BMTGPO>2.3.CO;2

24. Monaco CJ, Porporato EMD, Lathlean JA, Tagliarolo M, Sara G, McQuaid CD. Predicting the performance of cosmopolitan species: dynamic energy budget model skill drops across large spatial scales. Mar Biol. 2019;166: 14. doi:10.1007/s00227-018-3462-4

25. Monaco CJ, McQuaid CD. Applicability of Dynamic Energy Budget (DEB) models across steep environmental gradients. Sci Rep. 2018;8: 1–14. doi:10.1038/s41598-018-34786-w

26. Matzelle A, Montalto V, Sara G, Zippay M, Helmuth B. Dynamic Energy Budget model parameter estimation for the bivalve Mytilus californianus: Application of the covariation method. J Sea Res. 2014;94: 105–110. doi:10.1016/j.seares.2014.01.009

27. Boersch-Supan PH, Johnson LR. Two case studies detailing Bayesian parameter inference for dynamic energy budget models. J Sea Res. 2019;143: 57–69. doi:10.1016/j.seares.2018.07.014

28. Johnson LR, Pecquerie L, Nisbet RM. Bayesian inference for bioenergetic models. Ecology. 2013;94: 882–894. doi:10.1890/12-0650.1

694 29. Kearney M, Simpson SJ, Raubenheimer D, Helmuth B. Modelling the ecological niche
695 from functional traits. Philos Trans R Soc Lond B Biol Sci. 2010;365: 3469–83.
696 doi:10.1098/rstb.2010.0034

697 30. Harley CDG. Climate Change, Keystone Predation, and Biodiversity Loss. Science.
698 2011;334: 1124–1127. doi:10.1126/science.1210199

699 31. Meunier ZD, Hacker SD, Menge BA. Regime shifts in rocky intertidal communities
700 associated with a marine heatwave and disease outbreak. Nat Ecol Evol. 2024;8: 1285–
701 1297. doi:10.1038/s41559-024-02425-5

702 32. Helmuth BST, Hofmann GE. Microhabitats, Thermal Heterogeneity, and Patterns of
703 Physiological Stress in the Rocky Intertidal Zone. Biol Bull. 2001;201: 374–384.
704 doi:10.2307/1543615

705 33. Somero GN. The physiology of global change: linking patterns to mechanisms. Annu Rev
706 Mar Sci. 2012;4: 39–61. doi:10.1146/annurev-marine-120710-100935

707 34. Gillmor RB. Assessment of intertidal growth and capacity adaptations in suspension-
708 feeding bivalves. Mar Biol. 1982;68: 277–286. doi:10.1007/BF00409594

709 35. Petes LE, Menge BA, Harris AL. Intertidal Mussels Exhibit Energetic Trade-Offs
710 Between Reproduction and Stress Resistance. Ecol Monogr. 2008;78: 387–402.
711 doi:10.1890/07-0605.1

712 36. Khangaonkar T, Nugraha A, Xu W, Balaguru K. Salish Sea response to global climate
713 change, sea level rise, and future nutrient loads. J Geophys Res Oceans. 2019;124: 3876–
714 3904. doi:10.1029/2018JC014670

715 37. Sutton RT, Dong B, Gregory JM. Land/sea warming ratio in response to climate change:
716 IPCC AR4 model results and comparison with observations. Geophys Res Lett. 2007;34.
717 doi:10.1029/2006GL028164

718 38. Gilman SE, Wethey DS, Helmuth B. Variation in the sensitivity of organismal body
719 temperature to climate change over local and geographic scales. Proc Natl Acad Sci U S
720 A. 2006;103: 9560–9565.

721 39. King W, Sebens KP. Non-additive effects of air and water warming on an intertidal
722 predator–prey interaction. Mar Biol. 2018;165: 64. doi:10.1007/s00227-018-3320-4

723 40. Helmuth B, Mieszkowska N, Moore P, Hawkins SJ. Living on the Edge of Two Changing
724 Worlds: Forecasting the Responses of Rocky Intertidal Ecosystems to Climate Change.
725 Annu Rev Ecol Evol Syst. 2006;37: 373–404.
726 doi:10.1146/annurev.ecolsys.37.091305.110149

727 41. Bjelde BE, Todgham AE. Thermal physiology of the fingered limpet Lottia digitalis under
728 emersion and immersion. J Exp Biol. 2013;216: 2858–2869. doi:10.1242/jeb.084178

729 42. Althoff D, Filgueiras R, Brant Dias SH, Rodrigues LN. Impact of sum-of-hourly and daily
730 timesteps in the computations of reference evapotranspiration across the Brazilian
731 territory. Agric Water Manag. 2019;226: 105785. doi:10.1016/j.agwat.2019.105785

732 43. Bernhardt JR, Sunday JM, Thompson PL, O'Connor MI. Nonlinear averaging of thermal
733 experience predicts population growth rates in a thermally variable environment. Proc R
734 Soc B Biol Sci. 2018;285: 20181076. doi:10.1098/rspb.2018.1076

735 44. Denny M. The fallacy of the average: on the ubiquity, utility and continuing novelty of
736 Jensen's inequality. J Exp Biol. 2017;220: 139–146. doi:10.1242/jeb.140368

737 45. Montalto V, Sara G, Ruti PM, Dell'Aquila A, Helmuth B. Testing the effects of temporal
738 data resolution on predictions of the effects of climate change on bivalves. Ecol Model.
739 2014;278: 1–8. doi:10.1016/j.ecolmodel.2014.01.019

740 46. Bayne BL, Newell RC. 9 - Physiological Energetics of Marine Molluscs. In: Saleuddin
741 ASM, Wilbur KM, editors. The Mollusca. Academic Press; 1983. pp. 407–515.
742 doi:10.1016/B978-0-12-751404-8.50017-7

743 47. Fly EK, Hilbish TJ. Physiological energetics and biogeographic range limits of three
744 congeneric mussel species. Oecologia. 2013;172: 35–46. doi:10.1007/s00442-012-2486-6

745 48. Pousse E, Poach ME, Redman DH, Sennefelder G, White LE, Lindsay JM, et al. Energetic
746 response of Atlantic surfclam *Spisula solidissima* to ocean acidification. Mar Pollut Bull.
747 2020;161: 111740. doi:10.1016/j.marpolbul.2020.111740

748 49. Sebens KP. Energetic constraints, size gradients, and size limits in benthic marine
749 invertebrates. Integr Comp Biol. 2002;42: 853–61. doi:10.1093/icb/42.4.853

750 50. Wu RSS, Levings CD. An energy budget for individual barnacles (Balanus glandula). Mar
751 Biol. 1978;45: 225–235. doi:10.1007/bf00390605

752 51. Barillé L, Lerouxel A, Dutertre M, Haure J, Barillé A-L, Pouvreau S, et al. Growth of the
753 Pacific oyster (Crassostrea gigas) in a high-turbidity environment: Comparison of model
754 simulations based on scope for growth and dynamic energy budgets. J Sea Res. 2011;66:
755 392–402. doi:10.1016/j.seares.2011.07.004

756 52. Filgueira R, Rosland R, Grant J. A comparison of scope for growth (SFG) and dynamic
757 energy budget (DEB) models applied to the blue mussel (Mytilus edulis). J Sea Res.
758 2011;66: 403–410. doi:10.1016/j.seares.2011.04.006

759 53. Nisbet RM, Jusup M, Klanjscek T, Pecquerie L. Integrating dynamic energy budget
760 (DEB) theory with traditional bioenergetic models. J Exp Biol. 2012;215: 892–902.
761 doi:10.1242/jeb.059675

762 54. Rall BC, Vucic-Pestic O, Ehnes RB, Emmerson M, Brose U. Temperature, predator-prey
763 interaction strength and population stability. Glob Change Biol. 2010;16: 2145–2157.
764 doi:10.1111/j.1365-2486.2009.02124.x

765 55. Sanford E. Water temperature, predation, and the neglected role of physiological rate
766 effects in rocky intertidal communities. Integr Comp Biol. 2002;42: 881–891.
767 doi:10.1093/icb/42.4.881

768 56. Filgueira R, Chica M, Palacios JJ, Strohmeier T, Lavaud R, Agüera A, et al. Embracing
769 multimodal optimization to enhance Dynamic Energy Budget parameterization. Ecol
770 Model. 2020;431: 109139. doi:10.1016/j.ecolmodel.2020.109139

771 57. Wares JP, Cunningham CW. Diversification before the most recent glaciation in Balanus
772 glandula. Biol Bull. 2005;208: 60–68. doi:10.2307/3593101

773 58. Connell JH. A Predator-Prey System in the Marine Intertidal Region. I. Balanus glandula
774 and Several Predatory Species of Thais. Ecol Monogr. 1970;40: 49–78.
775 doi:10.2307/1942441

776 59. Bayne BL. Marine Mussels: Their Ecology and Physiology. Cambridge University Press;
777 1976.

778 60. Widdows J, Johnson D. Physiological energetics of Mytilus edulis: Scope for Growth. Mar
779 Ecol Prog Ser. 1988;46: 113–121. doi:10.2307/24827572

780 61. Palmer AR. A comparative and experimental study of feeding and growth in Thaidid
781 gastropods. University of Washington. 1980.

782 62. Gilman SE, Chen S, Wong JWH. Oxygen consumption in relation to body size, wave
783 exposure, and cirral beat behavior in the barnacle *Balanus glandula*. J Crustac Biol.
784 2013;33: 317–322.

785 63. Nishizaki MT, Carrington E. The effect of water temperature and velocity on barnacle
786 growth: Quantifying the impact of multiple environmental stressors. J Therm Biol.
787 2015;54: 37–46. doi:10.1016/j.jtherbio.2015.02.002

788 64. Ober GT, Rognstad RL, Gilman SE. The cost of emersion for the barnacle Balanus
789 glandula. Mar Ecol Prog Ser. 2019;627: 95–107. doi:10.3354/meps13058

790 65. Angilletta MJ. Estimating and comparing thermal performance curves. J Therm Biol.
791 2006;31: 541–545. doi:10.1016/j.jtherbio.2006.06.002

792 66. Ellington WR. The recovery from anaerobic metabolism in invertebrates. J Exp Zool.
793 1983;228: 431–444. doi:10.1002/jez.1402280305

794 67. Chan BKK, Hung OS. Cirral Length of the Acorn Barnacle Tetraclita Japonica
795 (Cirripedia: Balanomorpha) in Hong Kong: Effect of Wave Exposure and Tidal Height. J
796 Crustac Biol. 2005;25: 329–332. doi:10.1651/C-2535

797 68. Ritz DA, Crisp DJ. Seasonal Changes in Feeding Rate in Balanus-Balanoides. J Mar Biol
798 Assoc U K. 1970;50: 223-. doi:10.1017/S0025315400000734

799 69. Horn KM, Fournet MEH, Liautaud KA, Morton LN, Cyr AM, Handley AL, et al. Effects
800 of Intertidal Position on Metabolism and Behavior in the Acorn Barnacle, Balanus
801 glandula. Integr Org Biol. 2021;3: obab010. doi:10.1093/iob/obab010

802 70. Schneider CA, Rasband WS, Eliceiri KW. NIH Image to ImageJ: 25 years of image
803 analysis. Nat Methods. 2012;9: 671–675. doi:10.1038/nmeth.2089

804 71. Gilman S, Hayford H, Craig C, Carrington E. Body temperatures of an intertidal barnacle
805 and two whelk predators in relation to shore height, solar aspect, and microhabitat. Mar
806 Ecol Prog Ser. 2015;536: 77–88. doi:10.3354/meps11418

807 72. Fly EK, Monaco CJ, Pincebourde S, Tullis A. The influence of intertidal location and
808 temperature on the metabolic cost of emersion in Pisaster ochraceus. J Exp Mar Biol Ecol.
809 2012;422: 20–28. doi:10.1016/j.jembe.2012.04.007

810 73. Hill R, Wyse G, Anderson M. Animal Physiology, 3rd Edition. Sunderland, MA: Sinauer
811 Associates; 2008. Available: https://www.barnesandnoble.com/w/animal-physiology-3rd-
812 edition-richard-w-hill/1115655628

813 74. Sanford E, Menge B. Spatial and temporal variation in barnacle growth in a coastal
814 upwelling system. 2001;209: 143–157. doi:10.3354/meps209143

815 75. Roberts EA, Newcomb LA, McCartha MM, Harrington KJ, LaFramboise SA, Carrington
816 E, et al. Resource allocation to a structural biomaterial: Induced production of byssal
817 threads decreases growth of a marine mussel. Funct Ecol. 2021;35: 1222–1239.
818 doi:10.1111/1365-2435.13788

819 76. Harvey C. Effects of temperature change on demersal fishes in the California Current: A
820 bioenergetics approach. Can J Fish Aquat Sci. 2009;66: 1449–1461. doi:10.1139/F09-087

821 77. Helmuth B, Kingsolver JG, Carrington E. Biophysics, physiological ecology, and climate
822 change: does mechanism matter? Annu Rev Physiol. 2005;67: 177–201.
823 doi:10.1146/annurev.physiol.67.040403.105027

824 78. Joshi MM, Gregory JM, Webb MJ, Sexton DMH, Johns TC. Mechanisms for the land/sea
825 warming contrast exhibited by simulations of climate change. Clim Dyn. 2008;30: 455–
826 465. doi:10.1007/s00382-007-0306-1

79. Fly EK, Hilbish TJ, Wethey DS, Rognstad RL. Physiology and Biogeography: The Response of European Mussels (Mytilus spp.) to Climate Change*. Am Malacol Bull. 2015;33: 136–149. doi:10.4003/006.033.0111

80. Sokolova I. Bioenergetics in environmental adaptation and stress tolerance of aquatic ectotherms: linking physiology and ecology in a multi-stressor landscape. J Exp Biol. 2021;224: jeb236802. doi:10.1242/jeb.236802

81. Hesketh A, Harley C. Extreme heatwave drives topography-dependent patterns of mortality in a bed-forming intertidal barnacle, with implications for associated community structure. EcoEvoRxiv; 2022. doi:10.32942/osf.io/sn76j

82. Foster BA. Desiccation as a factor in intertidal zonation of barnacles. Mar Biol. 1971;8: 12–29. doi:10.1007/bf00349341

83. Connell JH. Community Interactions on Marine Rocky Intertidal Shores. Annu Rev Ecol Syst. 1972;3: 169–192.

84. Foulk A, Gouhier T, Choi F, Torossian JL, Matzelle A, Sittenfeld D, et al. Physiologically informed organismal climatologies reveal unexpected spatiotemporal trends in temperature. Conserv Physiol. 2024;12: coae025. doi:10.1093/conphys/coae025

85. Helmuth B, Broitman BR, Blanchette CA, Gilman S, Halpin P, Harley CDG, et al. Mosaic patterns of thermal stress in the rocky intertidal zone: Implications for climate change. Ecol Monogr. 2006;76: 461–479. doi:10.1890/0012-9615(2006)076[0461:MPOTSI]2.0.CO;2

86. Sanford E. The feeding, growth, and energetics of two rocky intertidal predators (Pisaster ochraceus and Nucella canaliculata) under water temperatures simulating episodic upwelling. J Exp Mar Biol Ecol. 2002;273: 199–218. doi:10.1016/S0022-0981(02)00164-8

87. Yamane L, Gilman SE. Opposite responses by an intertidal predator to increasing aquatic and aerial temperatures. Mar Ecol Prog Ser. 2009;393: 27–36. doi:10.3354/meps08276

88. Yee EH, Murray SN. Effects of temperature on activity, food consumption rates, and gut passage times of seaweed-eating Tegula species (Trochidae) from California. Mar Biol. 2004;145: 895–903. doi:10.1007/s00227-004-1379-6

89. Matzelle AJ, Sarà G, Montalto V, Zippay M, Trussell GC, Helmuth B. A Bioenergetics Framework for Integrating the Effects of Multiple Stressors: Opening a 'Black Box' in Climate Change Research*. Am Malacol Bull. 2015;33: 150–160. doi:10.4003/006.033.0107

90. George MN, Cattau O, Middleton MA, Lawson D, Vadopalas B, Gavery M, et al. Triploid Pacific oysters exhibit stress response dysregulation and elevated mortality following heatwaves. Glob Change Biol. 2023;29: 6969–6987. doi:10.1111/gcb.16880

91. Low-Décarie E, Boatman TG, Bennett N, Passfield W, Gavalás-Olea A, Siegel P, et al. Predictions of response to temperature are contingent on model choice and data quality. Ecol Evol. 2017;7: 10467–10481. doi:10.1002/ece3.3576

92. Padfield D, O'Sullivan H, Pawar S. rTPC and nls.multstart: A new pipeline to fit thermal performance curves in r. Methods Ecol Evol. 2021;12: 1138–1143. doi:10.1111/2041-210X.13585

93. Lorscheid I, Meyer M. Divide and conquer: Configuring submodels for valid and efficient analyses of complex simulation models. Ecol Model. 2016;326: 152–161. doi:10.1016/j.ecolmodel.2015.11.013

94. Lika K, Kearney MR, Freitas V, van der Veer HW, van der Meer J, Wijsman JWM, et al. The "covariation method" for estimating the parameters of the standard Dynamic Energy Budget model I: Philosophy and approach. J Sea Res. 2011;66: 270–277. doi:10.1016/j.seares.2011.07.010

95. Lika K, Kearney MR, Kooijman SALM. The "covariation method" for estimating the parameters of the standard Dynamic Energy Budget model II: Properties and preliminary patterns. J Sea Res. 2011;66: 278–288. doi:10.1016/j.seares.2011.09.004

96. Liang K-Y, Zeger SL. Inference Based on Estimating Functions in the Presence of Nuisance Parameters. Stat Sci. 1995;10: 158–173. doi:10.1214/ss/1177010028

97. Denny M. Buzz Holling and the Functional Response. Bull Ecol Soc Am. 2014;95: 200–203. doi:10.1890/0012-9623-95.3.200

98. Holling CS. Some Characteristics of Simple Types of Predation and Parasitism. Can Entomol. 1959;91: 385–398. doi:10.4039/Ent91385-7

99. Bayne BL, Hawkins AJS, Navarro E. Feeding and Digestion in Suspension-Feeding Bivalve Molluscs: The Relevance of Physiological Compensations1. Am Zool. 1988;28: 147–159. doi:10.1093/icb/28.1.147

100. Morton JE, Boney AD, Corner EDS. The adaptations of Lasaea rubra (Montagu), a small intertidal lamellibranch. J Mar Biol Assoc U K. 1957;36: 383–405. doi:10.1017/S0025315400016878

101. Newell RC, Pye VI, Ahsanullah M. Factors affecting the feeding rate of the winkle Littorina littorea. Mar Biol. 1971;9: 138–144. doi:10.1007/BF00348252

102. Dill LM, Gillett JF. The economic logic of barnacle Balanus glandula (Darwin) hiding behavior. J Exp Mar Biol Ecol. 1991;153: 115–127. doi:10.1016/S0022-0981(05)80010-3

103. Monaco CJ, Wethey DS, Helmuth B. A Dynamic Energy Budget (DEB) Model for the Keystone Predator Pisaster ochraceus. Plos One. 2014;9: e104658. doi:10.1371/journal.pone.0104658

104. Oliveira DF, Marques GM, Carolino N, Pais J, Sousa JMC, Domingos T. A multi-tier methodology for the estimation of individual-specific parameters of DEB models. Ecol Model. 2024;494: 110779. doi:10.1016/j.ecolmodel.2024.110779

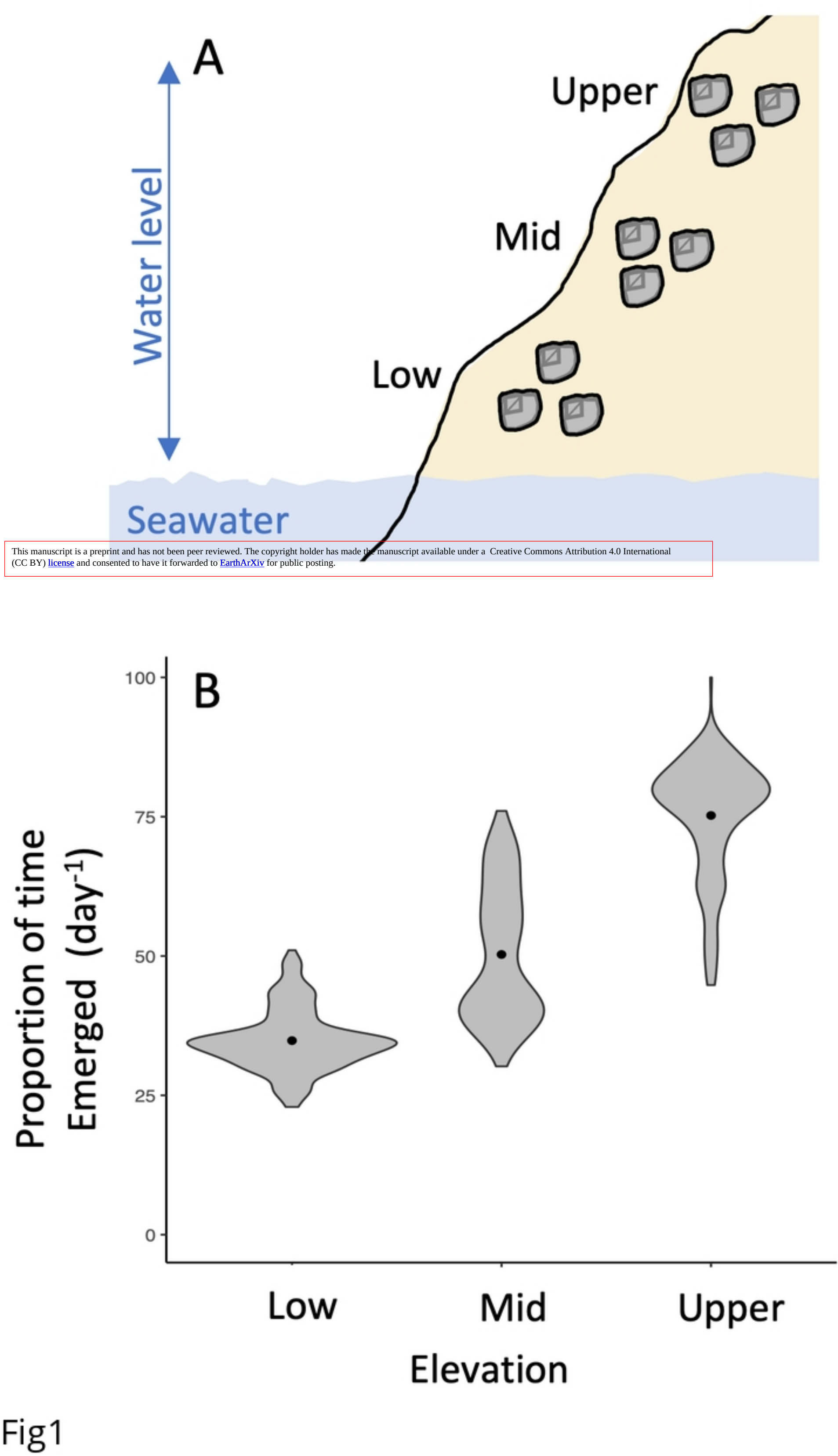

Fig1

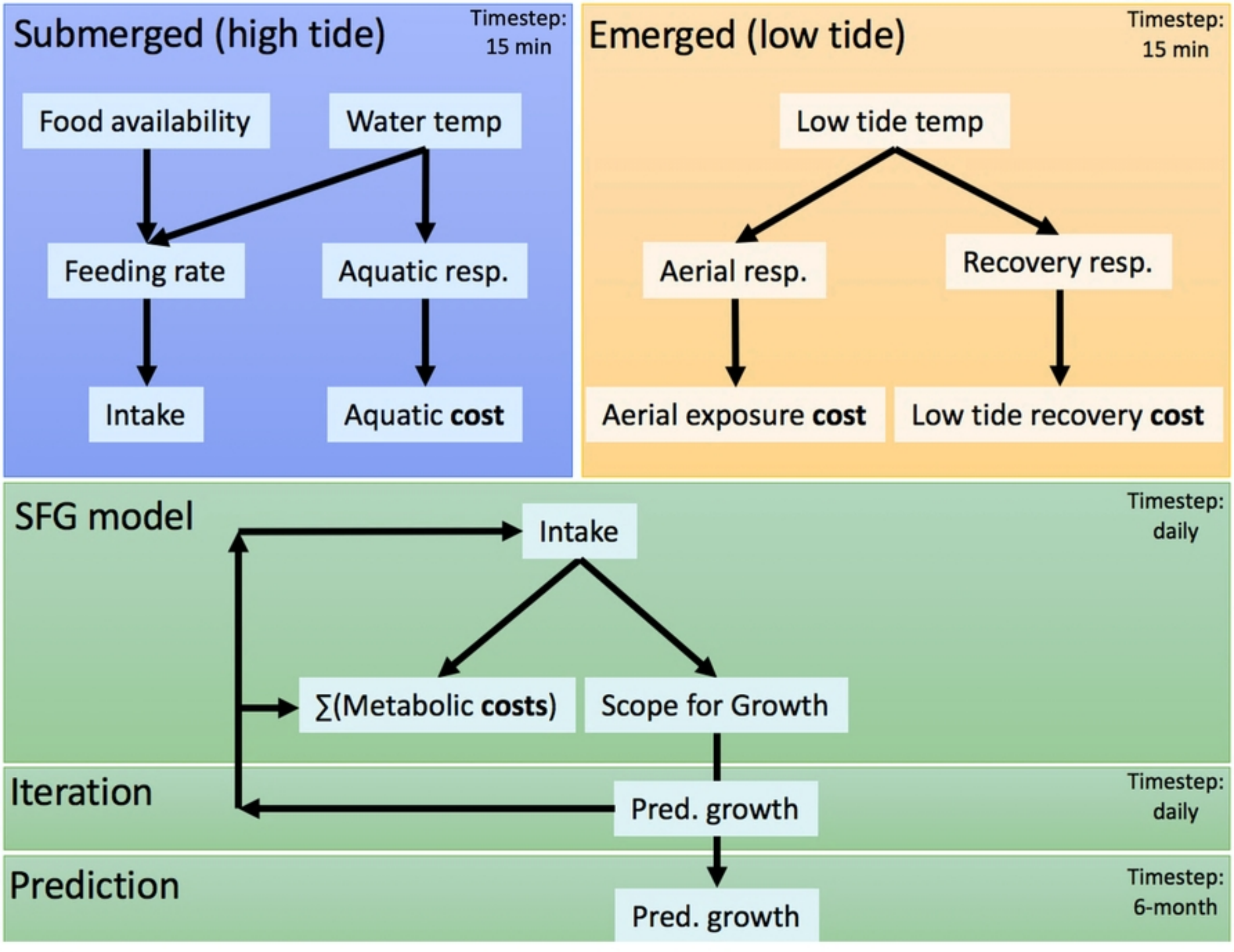
Submerged (high tide)
Timestep: 15 min
Food availability
Water temp
Feeding rate
Aquatic resp.
Intake
Aquatic cost
Emerged (low tide)
Timestep: 15 min
Low tide temp
Aerial resp.
Recovery resp.
Aerial exposure cost
Low tide recovery cost
SFG model
Timestep: daily
Intake
∑(Metabolic costs)
Scope for Growth
Iteration
Timestep: daily
Pred. growth
Prediction
Timestep: 6-month
Pred. growth

Fig2

Interval 1

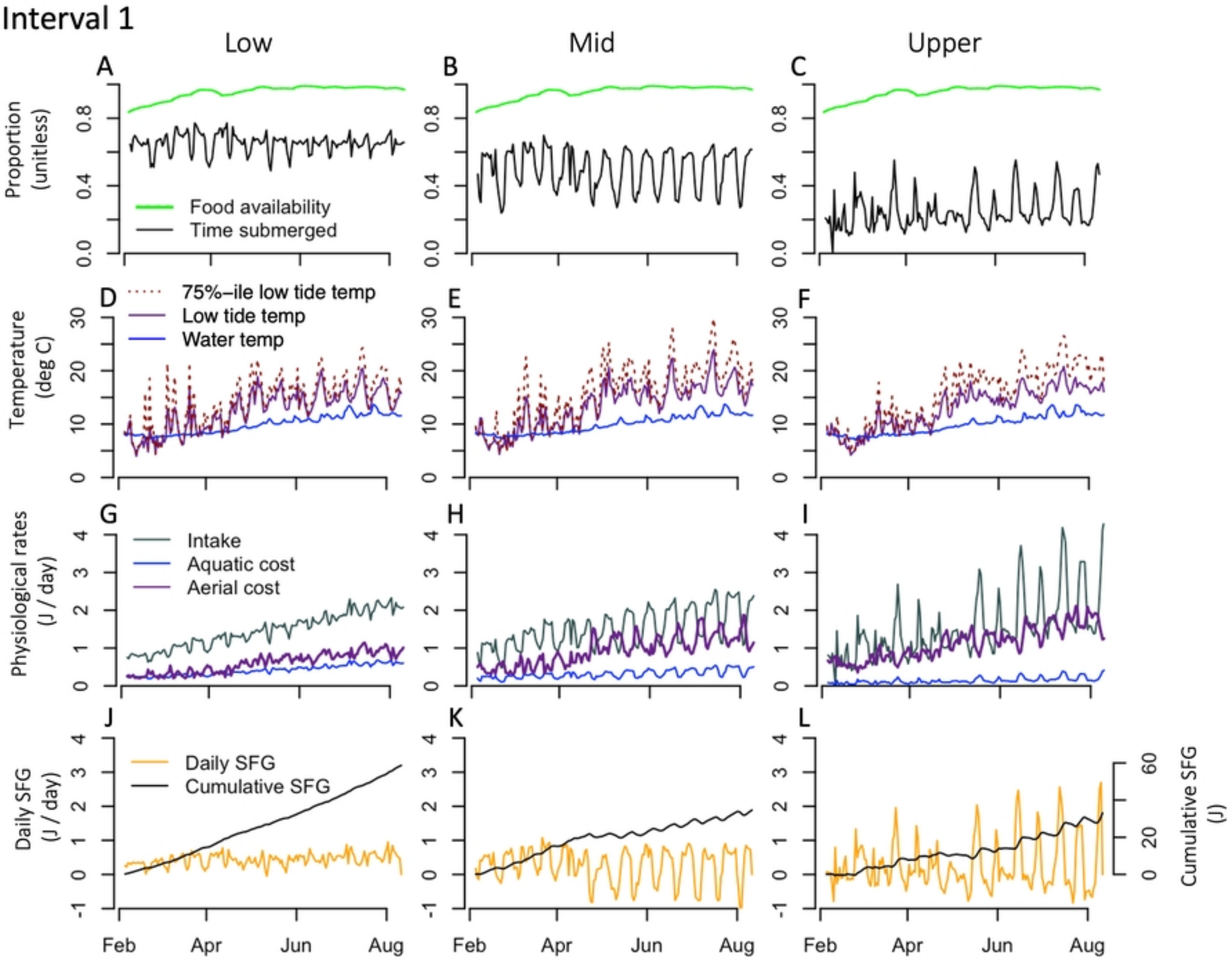

Fig3

Interval 2

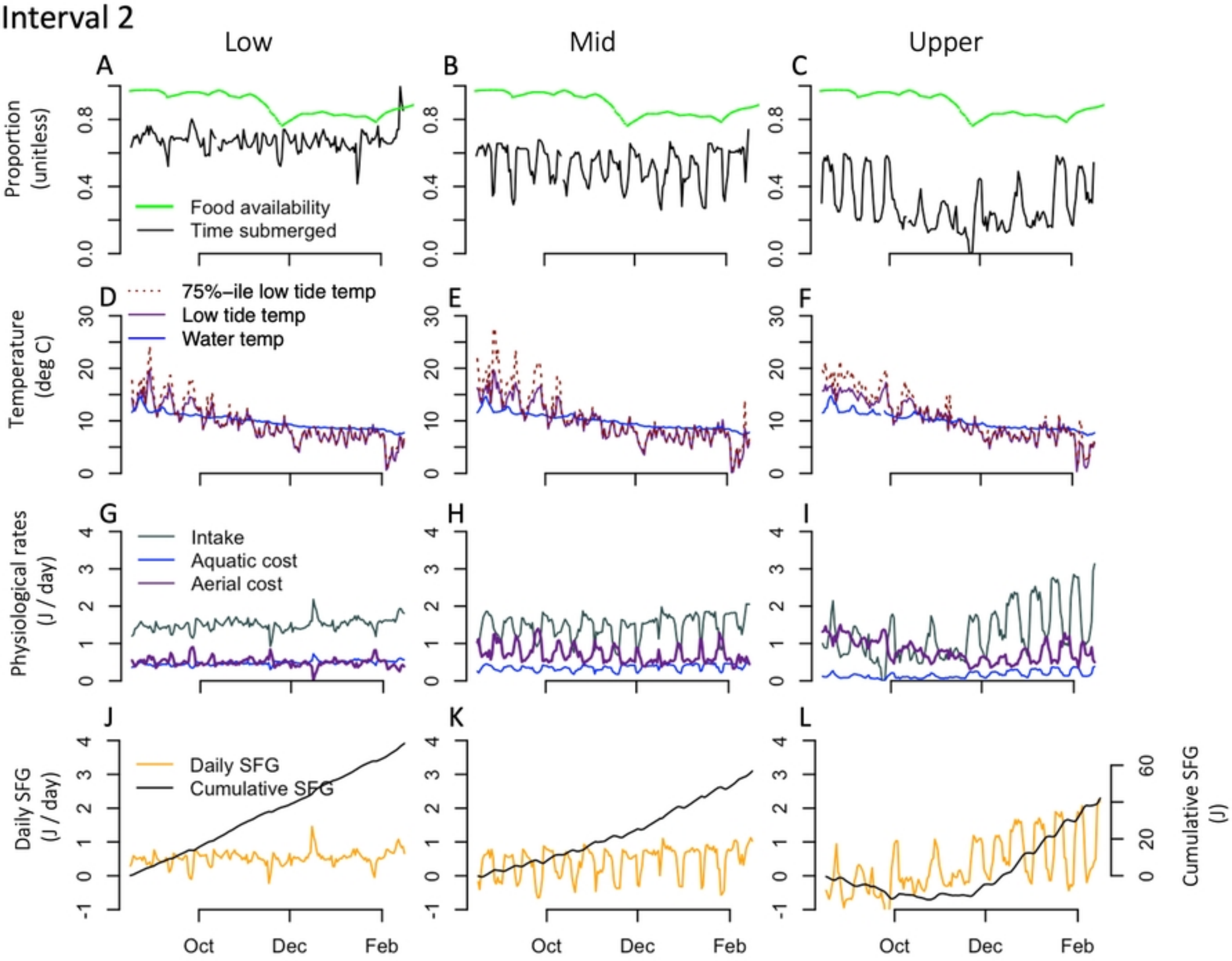

Fig4

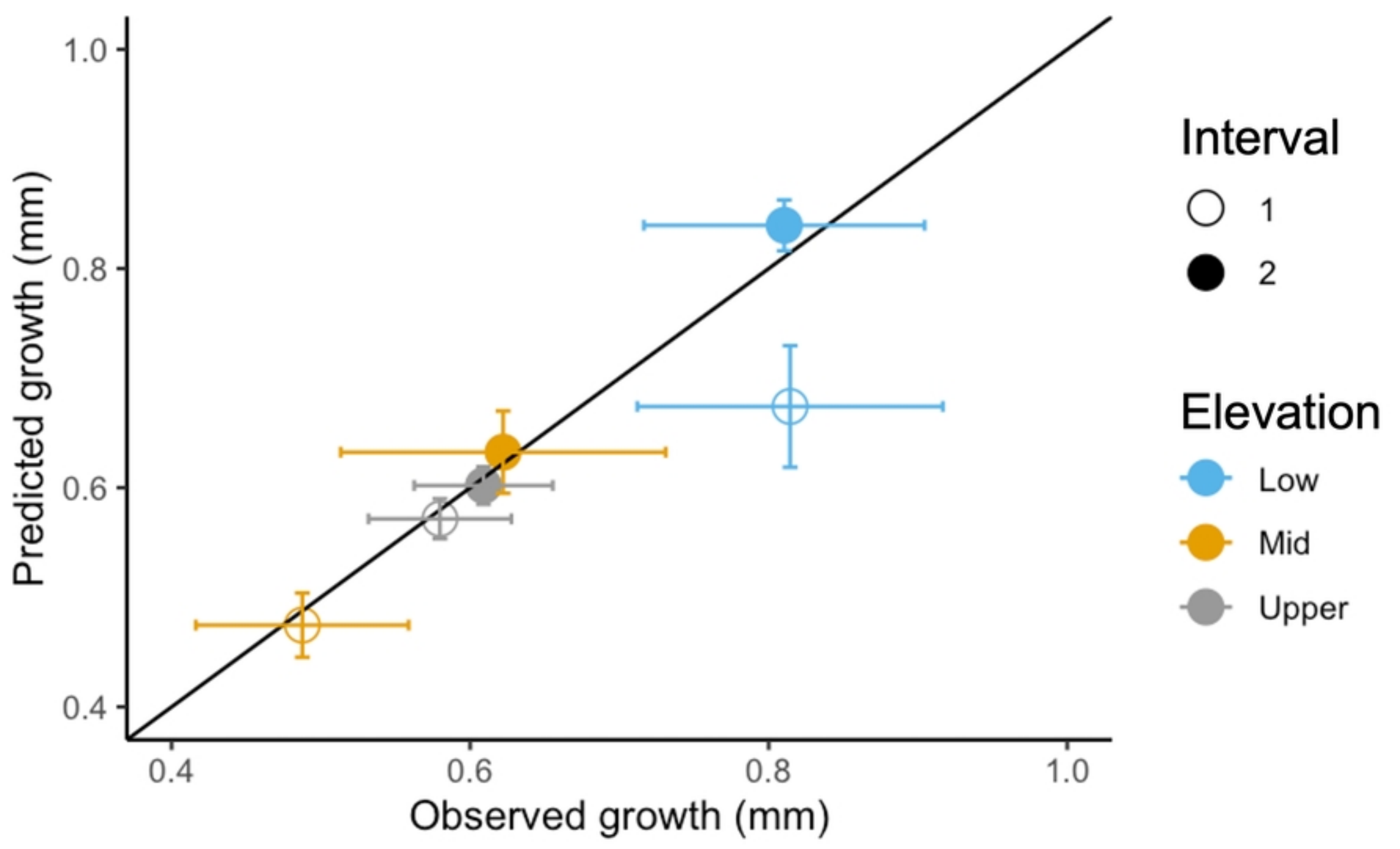
1.0
0.8
0.6
0.4
Predicted growth (mm)
0.4
0.6
0.8
1.0
Observed growth (mm)
Interval
1
2
Elevation
Low
Mid
Upper

Fig5

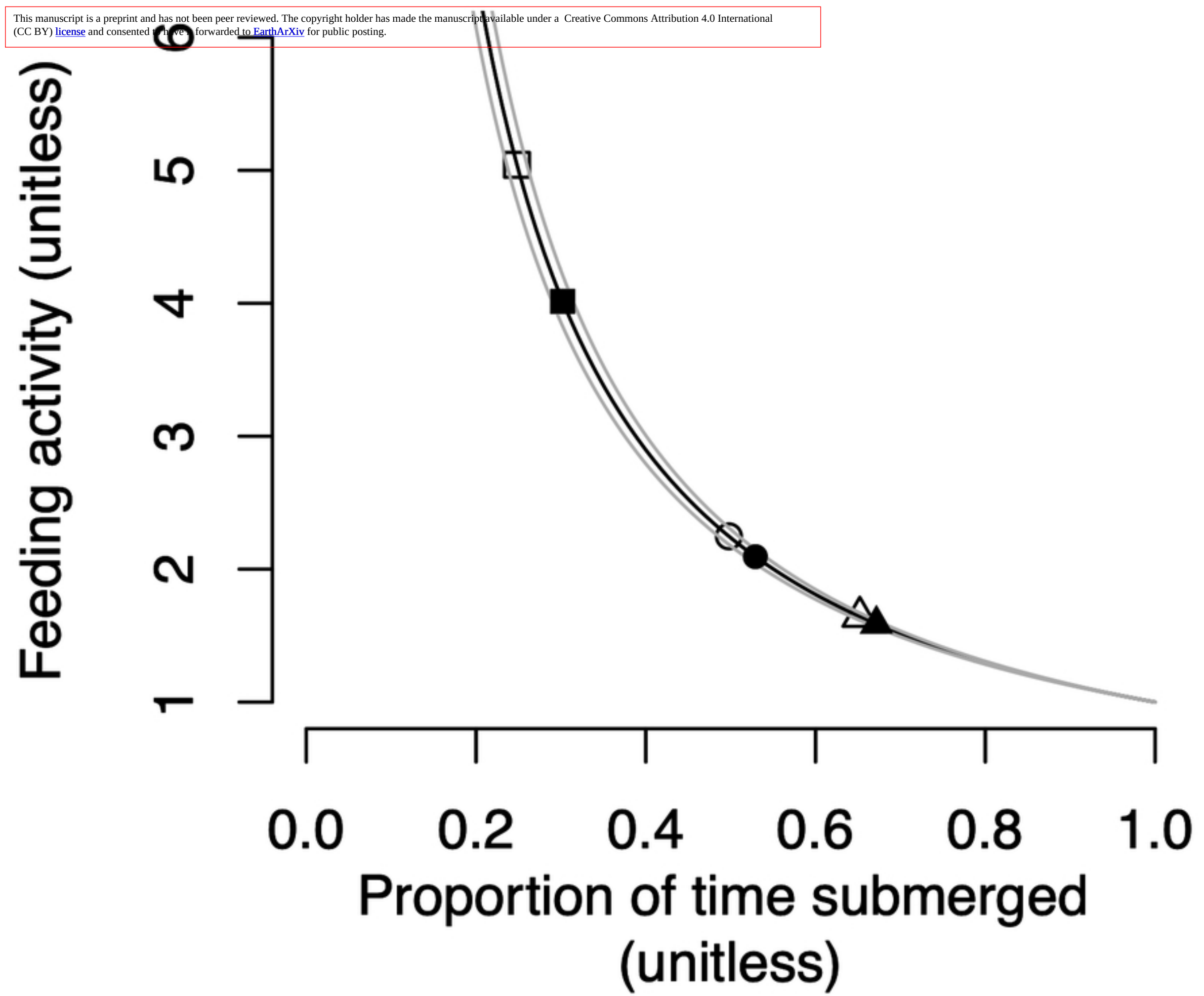

Fig6

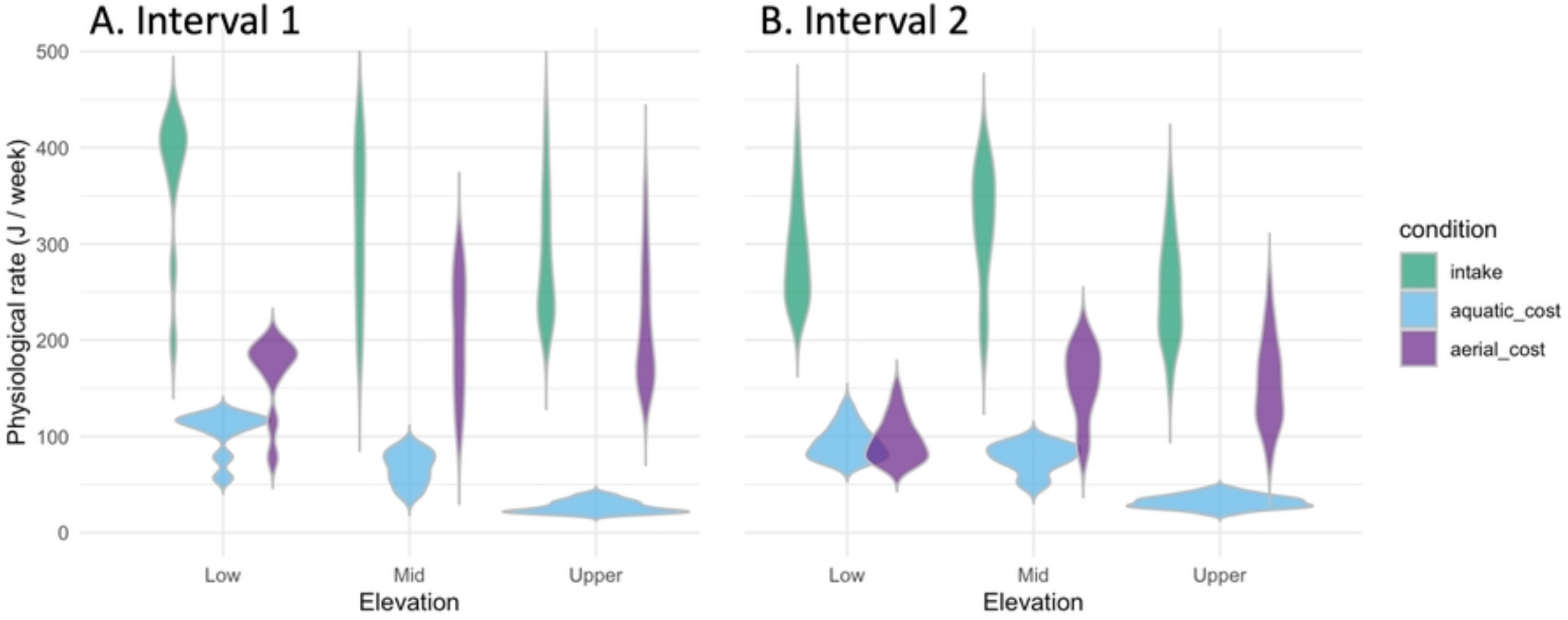
A. Interval 1
B. Interval 2
Physiological rate (J / week)
500
400
300
200
100
0
Low
Mid
Upper
Elevation
condition
intake
aquatic_cost
aerial_cost

Fig7

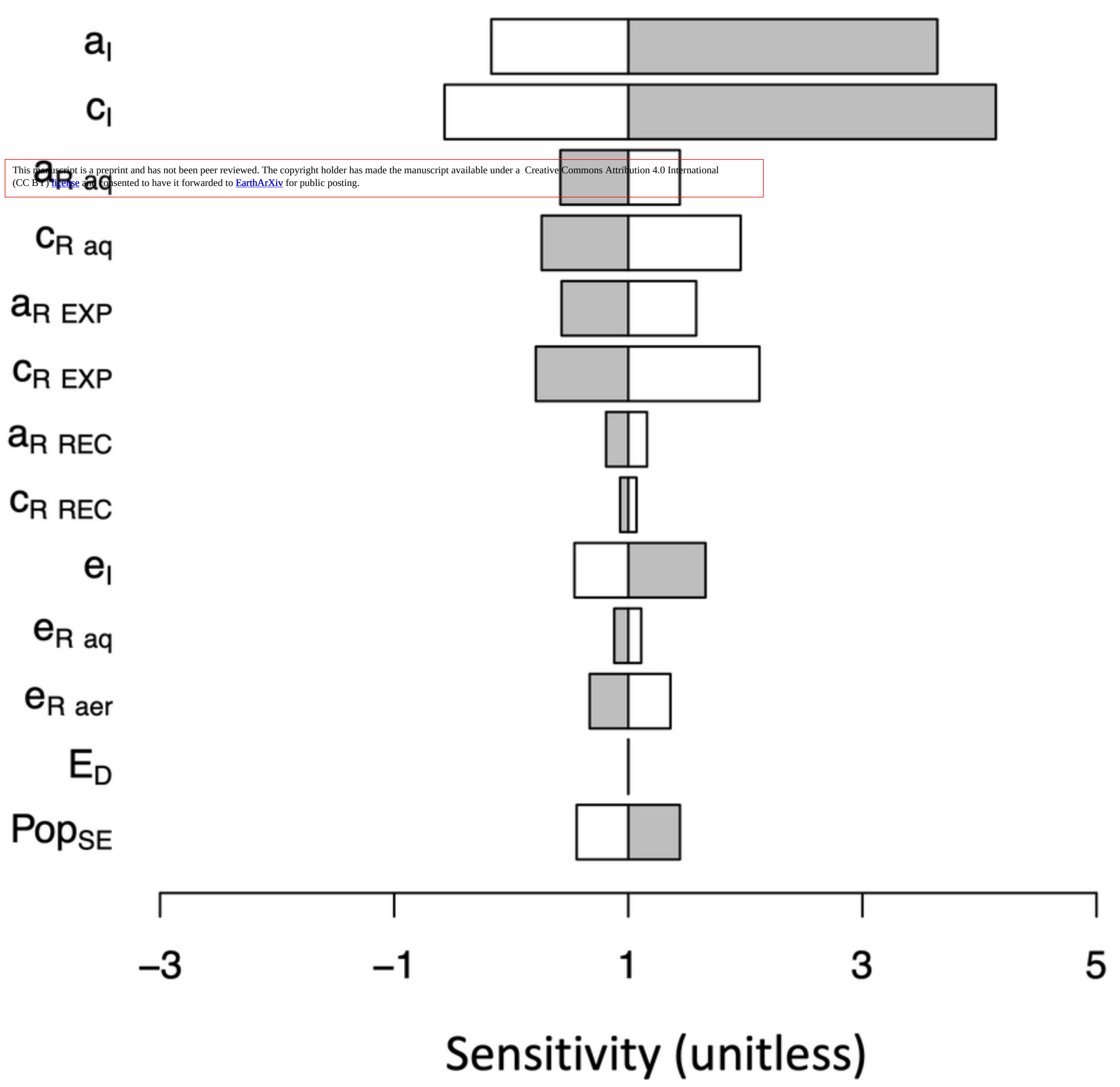

Fig8

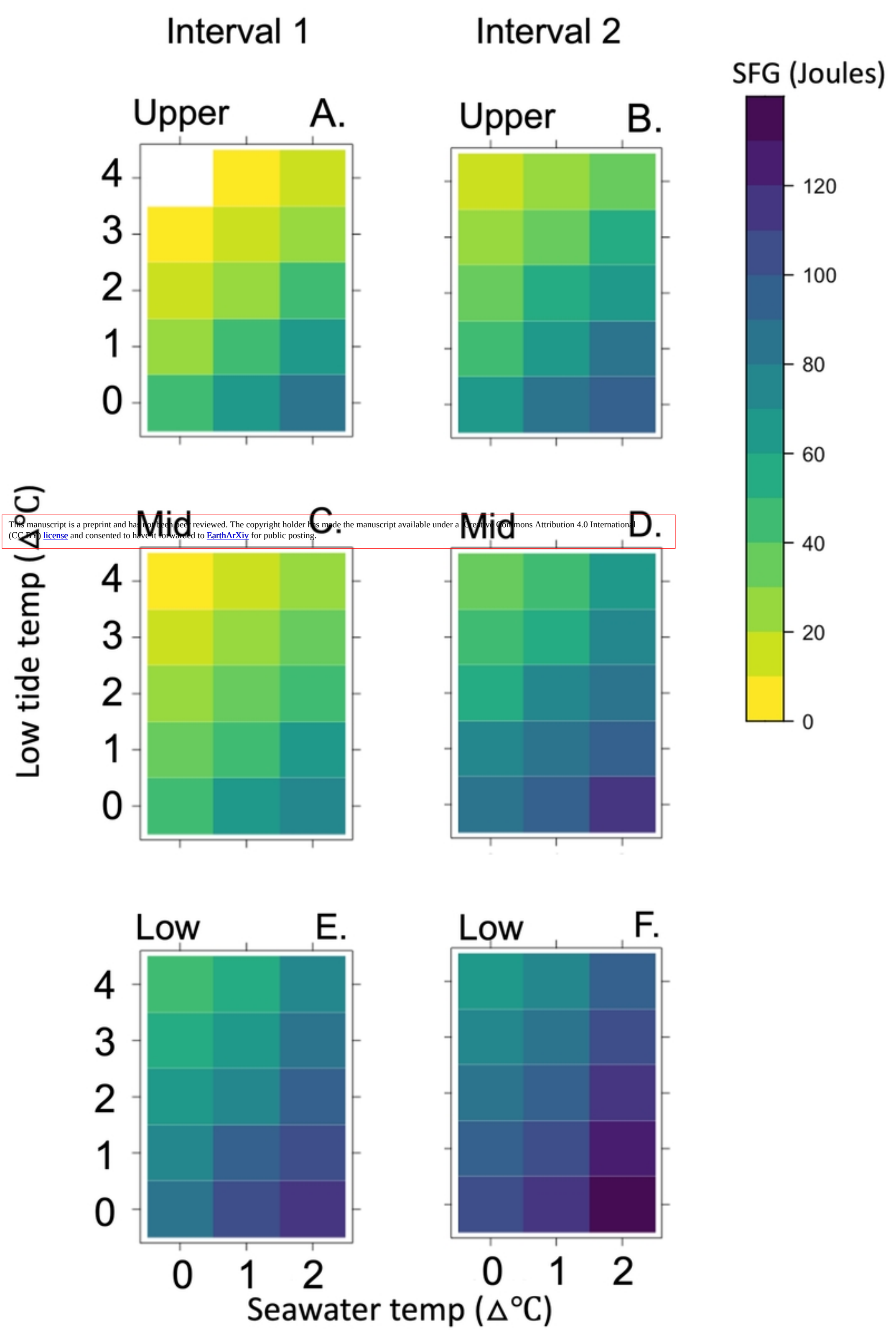

Fig9